

Coarse-grained vs. atomistic simulations: realistic interaction free energies for real proteins

Ali May^{1,2,*}, René Pool^{1,3,4,*}, Erik van Dijk¹, Jochem Bijlard¹, Sanne Abeln¹,
Jaap Heringa^{1,3} and K. Anton Feenstra^{1,3,†}

¹Centre for Integrative Bioinformatics (IBIVU) & Amsterdam Institute for Molecules Medicines and Systems (AIMMS), VU University Amsterdam, The Netherlands

²Department of Preventive Dentistry, Academic Centre for Dentistry Amsterdam (ACTA), University of Amsterdam and VU University Amsterdam, The Netherlands

³Netherlands Bioinformatics Centre (NBIC), Geert Groteplein 28, Nijmegen, The Netherlands

⁴Department of Biological Psychology, VU University Amsterdam, The Netherlands

Received on XXXXX; revised on XXXXX; accepted on XXXXX

Associate Editor: XXXXXXXX

ABSTRACT

Motivation: To assess if two proteins will interact under physiological conditions, information on the interaction free energy is needed. Statistical learning techniques and docking methods for predicting protein-protein interactions cannot quantitatively estimate binding free energies. Full atomistic molecular simulation methods do have this potential, but are completely unfeasible for large-scale applications in terms of computational cost required. Here we investigate whether applying coarse-grained (CG) molecular dynamics simulations is a viable alternative for complexes of known structure.

Results: We calculate the free energy barrier with respect to the bound state based on molecular dynamics simulations using both a full atomistic and a CG force field for the TCR-pMHC complex and the MP1-p14 scaffolding complex. We find that the free energy barriers from the CG simulations are of similar accuracy as those from the full atomistic ones, while achieving a speedup of over 500-fold. We also observe that extensive sampling is extremely important to obtain accurate free energy barriers, which is only within reach for the CG models. Lastly, we show that the CG model preserves biological relevance of the interactions: *i*) we observe a strong correlation between evolutionary likelihood of mutations and the impact on the free energy barrier with respect to the bound state; and *ii*) we confirm the dominant role of the interface core in these interactions. Our results therefore suggest that CG molecular simulations can realistically be used for the accurate prediction of protein-protein interaction strength.

Contact: k.a.feenstra@vu.nl

1 INTRODUCTION

Protein-protein interactions are at the heart of all processes in life. In order to understand living systems beyond the genome, comprehensive knowledge of protein-protein interactions (PPI) is therefore essential. Experimental techniques (Sprinzak *et al.*, 2003;

Kastritis and Bonvin, 2010; Ezkurdia *et al.*, 2009), prediction from sequence (Ezkurdia *et al.*, 2009), as well as protein-protein docking methods (Kastritis and Bonvin, 2010; Pons *et al.*, 2010) all have their specific limitations. To assess the likelihood of two proteins interacting under physiological interactions, we need to know both the concentrations and the dissociation constant (or binding free energy) of the proteins involved. Although it seems that the identification of the interface region is rather successful (Lensink and Wodak, 2010; Ofra and Rost, 2007), major open challenges are the accurate determination of interaction strength (Schueler-Furman *et al.*, 2005; Kastritis and Bonvin, 2010; Pons *et al.*, 2010), the incorporation of protein flexibility (Schueler-Furman *et al.*, 2005; Wollacott *et al.*, 2007; Tobi, 2010), and accounting for water and small solute entropic effects (Schueler-Furman *et al.*, 2005; Oshima *et al.*, 2011). Most importantly, Kastritis and Bonvin (2010) show that there is a poor correlation between binding affinity and scores for all nine commonly used docking algorithms they tested on 81 complexes with known binding affinity.

Molecular simulations using atomic pairwise interaction potentials are much more accurate for estimating interaction strength than docking scoring functions, though computationally much more expensive (Tuncbag *et al.*, 2009; Kastritis and Bonvin, 2010). Nevertheless, an immediate bonus of molecular simulation is that it addresses all three challenges mentioned above; interaction strength, flexibility, and entropic effects. For biomolecular simulation in general, the solvent (water) is the major obstacle to improve computational efficiency due to the large number of water molecules needed to solvate the protein. Many possible approaches to overcome this problem exist (for recent reviews, see Fennell and Dill, 2011; Dror *et al.*, 2012). Among the fastest available are the mean-field or *implicit solvent* methods, however one of the main drawbacks is the lack of accurate estimation of the solute entropy, especially in combination with charged solutes (Homeyer and Gohlke, 2012). By lumping together small molecules (e.g. water molecules) or molecular segments into ‘meta particles’, coarse-grained (CG) force fields do retain the explicit description of the system, *including* the solvent. Several CG models for water are available, each with their particular strengths and

*These authors contributed equally to this work

†To whom correspondence should be addressed

weaknesses (Hadley and McCabe, 2012). Compared to atomistic force fields, CG models provide increased computational efficiency at sufficient levels of accuracy (Tuffery and Derreumaux, 2012). For the calculation of molecular interactions, therefore, thermodynamic integration based on atomistic simulations with explicit water is both theoretically well founded and the most accurate solution available to date (Wereszczynski and McCammon, 2012).

In this work, we investigate the option of addressing the high computational cost of atomistic molecular simulations by the use of a CG force field for such simulations. For this, we will use the MARTINI CG protein force field for molecular dynamics (MD) simulations (Marrink *et al.*, 2007; Monticelli *et al.*, 2008). This force field was developed for CG simulations of biological membrane-protein systems, and has recently been used to simulate the spontaneous association of GPCR proteins in a lipid bilayer (Periole *et al.*, 2012). The MARTINI force field does not capture structural rearrangements, such as changes in secondary structure. We will assess its applicability and accuracy for the calculation of interaction strengths for a pair of protein structures in a water environment from constraint-force profiles.

By applying the MARTINI CG force field we first show that we are able to estimate the free energy barrier with respect to the bound state (ΔG^{off}) with similar accuracy compared to atomistic force field calculations and in good agreement with experimental data, but at more than 500-fold increased computational speed. For this we selected two test cases: a TCR-pMHC and an MPI-p14 scaffolding complex, both of which were previously studied with atomistic models (respectively Cuendet and Michelin, 2008; Cui *et al.*, 2008). We then show that calculated contributions of surface residues to the interaction strength are sensitive to changes in the amino acid residues involved. Random mutations at the interface core yield major changes in calculated interaction strengths, whereas mutations at the partially solvated interface rim only yield minor changes. Random mutations at the rest of the surface on average hardly affect the interaction strength at all. Moreover, we find that the evolutionarily most likely mutations, as assessed by standard residue exchange propensities, at the interface core also have a negligible influence on the interaction strength, whereas evolutionarily unlikely mutations disrupt favourable protein-protein interactions considerably. This behaviour with respect to mutations is consistent with what we would expect from a biological point of view. Finally, we discuss future implications of our finding that the major contributions to the interaction strength within our CG approach arise from the interface core.

2 METHODS

2.1 Software & force fields

The `mutate_model` script in Modeller (Sali and Blundell, 1993) was used to produce mutant structures. DSSP (Kabsch and Sander, 1983) and JOY (Mizuguchi *et al.*, 1998) were used to calculate the absolute and relative solvent accessibility of residues, respectively. VMD (Humphrey *et al.*, 1996) was used to visualise the structures.

We used GROMACS 4.0.5 (Hess *et al.*, 2008) for all MD simulations. Atomistic simulations were performed using the GROMOS G43a1 force field using the default time step ($\Delta t=1$ fs) (van Gunsteren *et al.*, 1996). CG simulations were performed using the MARTINI force field with the default time step ($\Delta t=20$ fs) (Marrink *et al.*, 2007). Coarse-graining (CG-ing) was

performed as previously described for the MARTINI model (Monticelli *et al.*, 2008). All 20 amino acids were mapped into four different bead types with respect to their physicochemical properties (SI Fig. 1). The non-bonded interactions between the CG solvent and solute particles were modelled by truncated and shifted Lennard-Jones pair-potential with a cutoff radius of 1.2 nm (Marrink *et al.*, 2007; Monticelli *et al.*, 2008).

2.2 The potential of mean force

We use the potential of mean force (PMF) to describe the interaction strength between two structures (Trzesniak *et al.*, 2007). The centre of mass (COM) separation r was chosen as the reaction coordinate along which the mean force is measured. Integration of the mean force along this pathway results in a free energy profile¹ that can be used to derive the free energy barrier with respect to the bound state ΔG^{off} . We first calculate the force F_{mean} as a function of the reaction coordinate from constrained MD simulations,

$$F_{\text{mean}}(r) = -\langle F_{\text{pull}}(r) \rangle_{NPT} = \frac{1}{2} \left\langle \left(\vec{F}_{\text{B}} - \vec{F}_{\text{A}} \right) \cdot \vec{r}_{\text{u}} \right\rangle_{NPT} \quad (1)$$

where $\langle F_{\text{pull}}(r) \rangle$ denotes the average force required to keep the interaction members at the constraint distance r , \vec{F}_{A} and \vec{F}_{B} the total forces acting on the first and the second interaction member which arise from direct interactions and interactions with explicitly simulated solvent, $\vec{r}_{\text{u}} = \vec{r}/r$ the unit vector connecting the two centres of mass, and angular brackets $\langle \dots \rangle_{NPT}$ an average in the isothermal-isobaric ensemble.

We define the constraint distance r as

$$r = |r_{\text{COM,A}} - r_{\text{COM,B}}| \text{ and } r \in \{r_1, r_2, \dots, r_N\}, \quad (2)$$

where $r_{\text{COM},i}$ is the COM position of interaction member i and N is the number of separation distances at which the F_{mean} values are calculated. Three arbitrary separations are illustrated in Fig. 1C for MPI-p14.

We calculated the F_{mean} at 50 distances for the TCR-pMHC (where $5 \text{ nm} \leq r \leq 7.45 \text{ nm}$) and at 54 distances for MPI-p14 ($2.16 \text{ nm} \leq r \leq 4.44 \text{ nm}$). In cases where we simulated nearly identical starting conformations of a particular structure for better sampling at distance r , we included these F_{mean} values into the average of $F_{\text{mean}}(r)$. After generating the force profile $F_{\text{mean}}(r)$ for the range of separations, we calculated the PMF by numerically integrating the interpolated $F_{\text{mean}}(r)$ as

$$\text{PMF}(r) = -\int_0^r dr' F_{\text{mean}}(r') \quad (3)$$

From this profile, the free energy barrier ΔG^{off} is obtained from the difference between the minimum of $\text{PMF}(r)$ at r_{min} and the maximum PMF value at larger distances $r > r_{\text{min}}$:

$$-\Delta G^{\text{off}} = \min[\text{PMF}(r)] - \max[\text{PMF}(r > r_{\text{min}})] \quad (4)$$

Errors in the forces are estimated from the standard deviations of the forces $\sigma_{F_{\text{mean}}}(r)$ across the set of replicate simulations at each distance r , and errors in the PMF $\sigma_{\text{PMF}}(r)$ are subsequently derived as follows:

$$\sigma_{\text{PMF}}(r) = \sqrt{\int_r^0 dr' \sigma_{F_{\text{mean}}}^2(r')} \quad (5)$$

2.3 Simulation setup

The wild-type (WT) X-ray structures of the TCR-pMHC (Garboczi *et al.*, 1996) and MPI-p14 (Kurzbaue *et al.*, 2004) complexes, resolved respectively at 2.6 Å and 1.9 Å, were taken from the Protein Data Bank entries 1ao7 and 1vet. The TCR-pMHC structure contains 707 residues, of the human A6 TCR in complex with the MHC-bound Tax nanopptide. The MPI-p14 complex contains 240 residues, of two structurally very similar chains of low sequence similarity, with a large and shallow interface.

¹ Strictly, the PMF is not a free energy profile as it does not correct for standard conditions; this is covered in the Supporting Information.

Equilibration procedure For the atomistic and CG simulations, a general equilibration scheme was performed, which was identical for atomistic and CG except where noted below. First, the structure was energy minimised in vacuum, followed by the separation of the interacting proteins to the constraint distance r along the reaction coordinate. These structures, for each r , were solvated in a periodic cubic box with a size ensuring a minimum distance between the proteins and the box edges to avoid self-interactions with periodic images. For the atomistic simulations, the SPC water model and a minimum distance of 1.2 nm were used. For the CG simulations, MARTINI water was used with a 1.0 nm minimum distance. Energy minimisation on the solvated system was performed first with and then without position restraints. In the atomistic energy minimisation, position restraints were first put on non-H atoms, followed by restraining only C_α atoms. The system was neutralised by adding as many Na^+ or Cl^- counter ions as needed for a total charge of zero. Then, another unrestrained energy minimisation was performed. The neutralised and solvated structure was simulated for 20 ps (atomistic) or 30 ps (CG) with position restraints on the C_α atoms (atomistic) or whole structure (CG), to allow the solvent to equilibrate around the solute. The temperature was set to $T=303$ K using a Berendsen (Berendsen *et al.*, 1984) (CG) or Nosé-Hoover (Cheng and Merz, 1996) (atomistic) thermostat with $\tau_T=0.1$ ps. The pressure in atomistic simulations was set to $P=1$ bar using a Parrinello-Rahman barostat (Parrinello and Rahman, 1981) with $\tau_P=0.5$ ps. In CG simulations, pressure was set to $P=300$ bar², using a Berendsen barostat (Berendsen *et al.*, 1984) with $\tau_P=0.5$ ps. Temperature and pressure were equilibrated for 0.1 ns (atomistic) or 0.2 ns (CG). The resulting conformations were used in the production simulations without position restraints.

Atomistic production simulations. Atomistic production MD simulations were performed for the WT TCR-pMHC (3 replicates) and MP1-p14 (10 replicates). Equilibration procedure and production runs were repeated for each distance (Eq. 2). Each production simulation was run for 2 ns.

Coarse-grained production simulations. CG production MD simulations were performed for the WTs and *in-silico* mutants (20 replicates). Before starting the CG equilibration procedure, the atomistic structure was first energy minimised and then was coarse-grained using `atom2cg` (<http://md.chem.rug.nl/cgmartini>). The tertiary structure of the CG complex was stabilised by generating distance restraints on the backbone atoms (cf. Marrink *et al.*, 2007). This equilibration procedure and the production runs were repeated for each distance in Eq. 2. Production simulations were run for 2 ns or 2 μs as indicated.

2.4 Definition of different residue classes

The relative and absolute solvent accessible surface area (SASA) of the residues were calculated in the monomer (e.g. TCR) and dimer form (e.g. TCR-pMHC). Subsequently, residues that have $<7\%$ of their side chain accessible to the solvent in both forms were defined as protein core. Residues that have $>7\%$ of their side chain exposed to the solvent in the monomer and $<7\%$ in the dimer were defined as interface core. Residues that have $>7\%$ of their side chain accessible to the solvent in both forms were defined as interface rim if there was a difference of at least 1 \AA^2 in their absolute SASA between two forms. Residues that do not fall into one of the above groups were called surface (S) residues. The outer interface rim class is composed of the closest surface residue neighbours of interface rim residues located on the same monomer. The number of outer rim residues identified in a complex is the same as the number of rim residues.

2.5 In silico mutations & statistical analysis

To probe the biological relevance of the CG calculations, we introduce mutations guided by the BLOSUM62 substitution matrix (Henikoff and

Henikoff, 1992), in the MP1-p14 complex. We mutated all 23 interface core residues to the amino acid with the highest substitution score (other than itself) to obtain the evolutionarily most likely mutant (see SI Table 6). In a separate set of mutations, we mutated the interface core to the lowest-scoring substitutions to obtain the least likely mutant (see SI Table 6). We performed 20 replicate simulations for both mutants, each starting from slightly different starting conformations. Next, we also made all 23×19 possible interface core mutants, and simulated each 10 times.

To further probe biological relevance, we compare the effects of random mutations at different locations at and around the interface for both the MP1-p14 and the TCR-pMHC complex. We created 20 compositionally different interface core mutants where all n interface core residues (see SI Table 2) were substituted with randomly chosen amino acids. Then, we created 20 different interface rim mutants by randomly substituting n interface rim residues with random amino acids. Next, we obtain 20 outer interface rim mutants by randomly substituting the n non-interface neighbours of the interface rim. We calculated the PPI for each of these mutants only once rather than multiple replicates. Differences in the free energy barrier $\Delta\Delta G$ were statistically tested with a two-sided Mann-Whitney test, separately for every mutant and for the WT.

Finally, we made specific interface mutations in a homologue of the TCR-MHC complex described by Wu *et al.* (2002). We chose the 7 mutants with the largest measured $\Delta\Delta G$ s: in the β chain Q64A, E69A and A73G, and in the peptide K99R, T102N, T102S and the double mutant Y97F/T102S.

3 RESULTS

Calculation of free energy barrier with respect to the bound state

In order to obtain the free energy barriers to compare atomistic and CG results, we calculate the potential of mean force (PMF, Fig. 1C & D). This can be derived from the mean force F_{mean} (Eq. 1) required to constrain interaction members (e.g. TCR and pMHC) at a number of centre of mass separation distances (Fig. 1A & B).

Several immediate observations can be drawn from Fig. 1. First, force profiles obtained by the atomistic and the CG model are in reasonable agreement for both complexes (Fig. 1A & B). Second, at a given separation distance r , simulations of nearly identical starting conformations (identical symbols in Fig. 1A & B on the distance r) yield a distribution of force values in both atomistic and CG simulations rather than converging to some value. Last, these distributions overlap closely for distances larger than ~ 2.75 nm (Fig. 1A) and ~ 5.5 nm (Fig. 1B), but diverge at shorter distances.

Next we calculated the average mean force at each distance to obtain the force profiles $F_{\text{mean}}^{\text{atom}}(r)$, in blue, and $F_{\text{mean}}^{\text{CG}}(r)$, in green in Fig. 1A & B. We calculated the PMF by numerically integrating the interpolated $F_{\text{mean}}(r)$ cf. Eq. 3 (Fig. 1C & D). The free energy barrier can now simply be obtained from the well-depth of the PMF, cf. Eq. 4. The resulting PMFs shown in Fig. 1C & D for both complexes provide a comparison between the free energy minima calculated from the atomistic and the CG simulations, as well as with the experimentally determined interaction strengths.

For the MP1-p14 complex, atomistic and CG simulations yielded free energy barriers $\Delta G^{\text{off}}=132$ and 104 kJ mol^{-1} respectively, both overestimating the reported experimental $\Delta G^{\text{off}}=91 \text{ kJ mol}^{-1}$ (Kurzbaue *et al.*, 2004). For the TCR-pMHC complex, atomistic and CG simulations yielded free energy barriers $\Delta G^{\text{off}}=101$ and 80 kJ mol^{-1} respectively, very close to the experimental values $\Delta G^{\text{off}}=79.5 \text{ kJ mol}^{-1}$ (Ding *et al.*, 1999) and $\Delta G^{\text{off}}=78.6 \text{ kJ mol}^{-1}$ (Davis-Harrison *et al.*, 2007). See SI Table 1 for further details. Note that a very small correction

² The high pressure in the CG simulations was applied to ensure the bulk MARTINI CG water is in the fluid region of the phase diagram. We determined the MARTINI CG water phase diagram from separate Gibbs ensemble simulations (Frenkel and Smit, 2002).

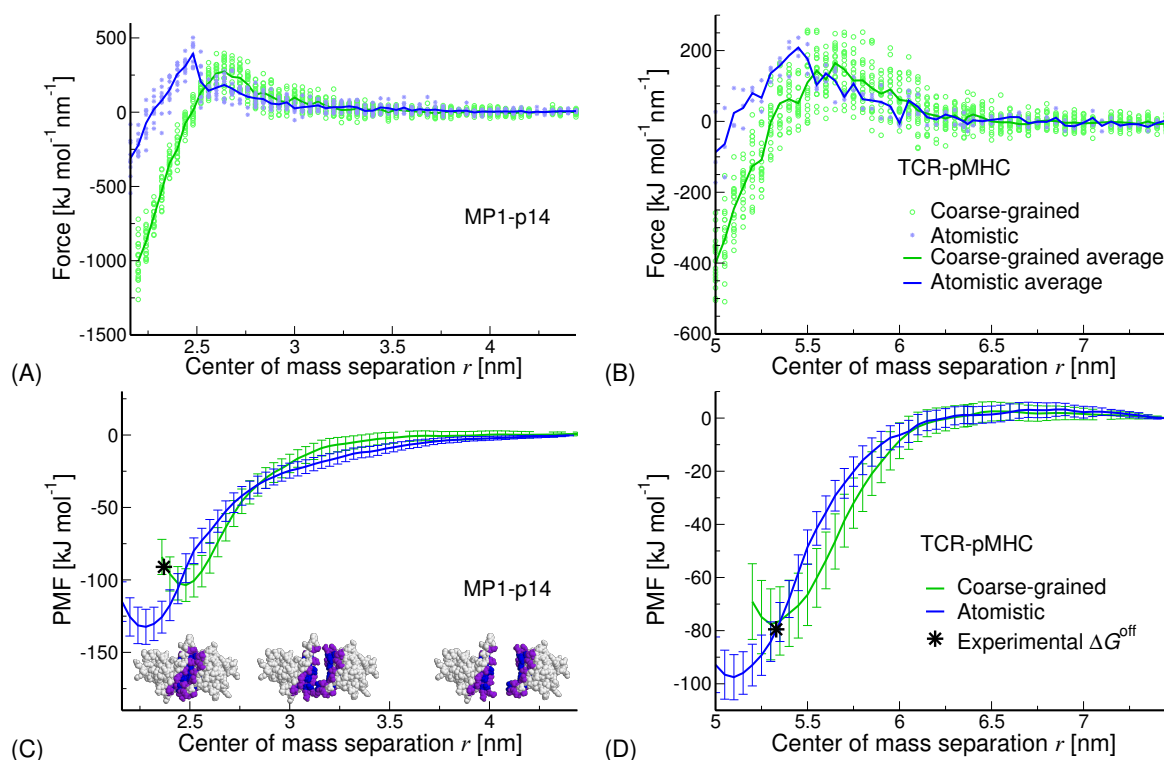


Fig. 1. The mean force profile and the PMF from atomistic and CG calculations. (Top) Identical symbols at a given distance are calculations of the mean force from simulations that differ slightly in their starting conformations. Blue and green lines describe the means of these values at each distance, respectively for atomistic and CG simulations. (Bottom) Potential of mean force describing the free energy of dissociation. Distances more than 1 Å below the PMF minimum are not shown. Blue and green lines describe the PMF obtained by atomistic and CG simulations, respectively. The corresponding free energy profiles are shown in SI Fig. 3. Stars show experimentally determined ΔG^{off} and equilibrium distances in the native crystal structures. Error bars are based on standard deviations in the mean force cf. Eq. 5. (A & C) MP1-p14 and (B & D) TCR-pMHC complex.

must be made to the free energy barrier (Gilson *et al.*, 1997) which amounts to ~ 4 kJ mol⁻¹, see SI for a detailed calculation. In order to probe the effect of sampling of the rotational degrees of freedom, for the MP1-p14 complex we also calculated the PMF based on a triplicate set of long 2 μ s CG simulations. SI Fig. 4 shows ordering is present in the short (2 ns) simulations, as well as at close distances in the long (2 μ s) simulations, however this ordering disappears at farther distances (>4 nm) in the long simulations, indicating a strongly improved rotational sampling. We found a negligible change in the ΔG^{off} as a result of this improved sampling.

Besides interaction strength, Fig. 1C & D present a comparison between the experimentally reported PPI equilibrium distance (the separation distance in X-ray structure) and the corresponding value from simulations (the distance at the PMF minimum). We see that the experimental distances were slightly underestimated by the atomistic PMF in both cases, while the CG PMF appears to yield distances closer to the crystal structure, especially in the case of TCR-pMHC interaction.

Computational speed-up

The running time of atomistic MD simulations for MP1-p14 at the longest COM separation distance $r=4.44$ nm was 284 CPU-hours. CG-ing reduced the running time at this distance to 0.5 CPUh, yielding a 568-fold speed-up. Shorter separations are progressively

faster, but show similar speed-ups. In the case of the TCR-pMHC, this was 1333 and 2.5 CPUh, respectively, for a speed-up of 533-fold. In total, we invested well over 300 000 CPUh in the atomistic simulations, over the three and 10 replicate calculations for the TCR-pMHC and MP1-p14 complexes, respectively. In contrast, the CG simulations for the 456 different mutants (10 or 20 replicates each), only required about 100 000 CPUh. The 2 μ s CG simulations (three replicates) required an additional 64 000 CPUh.

Evolutionary likelihood of mutations and the free energy

To obtain a simple, though biologically relevant test case, we substituted interface core residues in MP1-p14 according to BLOSUM62 (Henikoff and Henikoff, 1992). We define two sets of mutations; one where each residue is mutated into the evolutionarily most distant residue, and one where it is mutated into the closest residue type (detailed substitutions in SI Table 6). One would expect minimal distortion of the PMF from the closest substitutions, and maximal distortion for the evolutionarily most distant substitutions.

It is clear from results shown in Fig. 2A that when the interface core composition was altered with the most similar amino acids, change in the interaction strength remains insignificant ($\Delta\Delta G^{\text{off}}=7$ kJ mol⁻¹, $p<.38$; see SI Table 5 for detailed significance values), whereas substitutions with the most dissimilar amino acids have a strongly disruptive effect on the PPI

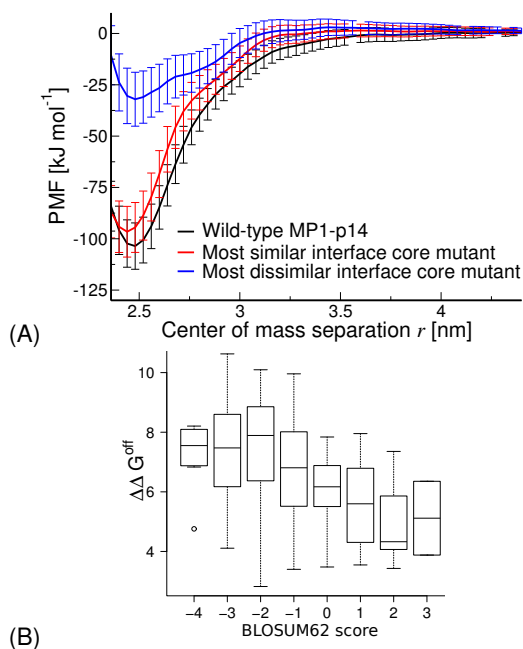


Fig. 2. The PPI effects of different mutations at the MP1-p14 interface. (A) PMF curves of the WT, the most similar and dissimilar mutants in black, red and blue, respectively. Error bars are based on standard deviations in the mean force cf. Eq. 5. (B) Box-plot of average $\Delta\Delta G^{\text{off}}$ per substitution type, based on pairwise differences between single mutations at the interface core, vs. the corresponding BLOSUM62 substitution score, with a correlation $R = -0.39$ and significance $p \leq 2.2 \cdot 10^{-8}$.

that is highly significant ($\Delta\Delta G^{\text{off}} = 71.5 \text{ kJ mol}^{-1}$, $p < 10^{-11}$; see SI Table 5). However, we still observe a favourable interaction ($\Delta G^{\text{off}} = 32 \pm 13 \text{ kJ mol}^{-1}$) with the most dissimilar mutant structure. Note, that the force field alone has no such predictive value (see SI Fig. 7).

We have in addition considered all single mutations for each of the 23 interface core residues for MP1-p14. Of all $\Delta\Delta G^{\text{off}}$ s with respect to the WT, 16 are significant ($p \leq 0.05$ using Student's t -test with Hommel multiple testing correction; 121 at $p \leq 0.05$ with just t -test). This corresponds to a detection limit of about $\Delta\Delta G^{\text{off}} \geq 8 \text{ kJ mol}^{-1}$. Fig. 2B compares $\Delta\Delta G^{\text{off}}$ between all mutants (excluding the WT as the rest of the protein structure is biased towards the WT amino acid) with the corresponding BLOSUM62 scores, and shows that there is a strong correlation between them, as expected. In a homologue of the TCR-pMHC complex, we furthermore show that we can reproduce experimental ΔG^{off} s for interface mutations to within the accuracy of our calculations (see SI Fig. 7).

The interface core dominates the interaction

Our final *in-silico* experiment with the CG model was aimed at investigating the effective role of interface residues in the interaction between two proteins. We first defined classes of residues based on solvent accessible surface area and distance (Fig. 3, for definitions see Methods, a summary is provided in SI Table 2).

We substituted the same number of residues from each class with randomly chosen amino acids, and calculated the interaction

strength in the resulting mutant complexes. The resulting PMFs shown in Fig. 4 indicate significant disruptive effects of mutations at the interface core in both the MP1-p14 ($p < 10^{-8}$; see SI Table 3 for detailed significance values) and TCR-pMHC ($p < 2 \cdot 10^{-4}$; see SI Table 4), whereas mutations in the the interface rim appear to have very little influence on the PMF compared to the WT. Note that in both complexes mutations of outer rim sometimes yielded enhanced interaction strengths.

4 DISCUSSION & CONCLUSION

In this paper, we have set out to answer the following questions. First, can we use CG MD simulations to get the free energy barrier with respect to the bound state for protein-protein interactions that are of similar accuracy to those from atomistic MD simulations? Second, what is the gain in speed and overall sampling for CG versus atomistic? Lastly, can we get biologically relevant results from the CG model, similar to what we expect to get from the atomistic model (at much higher computational cost)?

Biological relevance

We have shown that by using the CG MARTINI force field, we obtain free energy barriers that are at least as close to the experimental values as those obtained using an atomistic force field. Moreover, evolutionarily least likely mutations, according to BLOSUM62 substitution propensities, at the interface core disrupt binding, while the most likely mutations hardly influence binding. It is important to note here that the residue similarities from large-scale sequence comparisons, as captured in the BLOSUM62 matrix, are independent of the MARTINI CG force field.

Likewise, mutations on the interface core have a much more disruptive effect on the binding than those at the interface rim. Mutations farther away from the interface have negligible effects. This is consistent with findings that residues at the interface core in general behave much like protein core, while interface rim residues are more similar to those at the surface (e.g., Tuncbag *et al.*, 2009). These results show that the CG MARTINI force field is sensitive to changes in the shape and physicochemical properties of the interface, and suggest it is suitable for studying the effects of biologically relevant structural changes in PPIs.

Of note, we observe that even the evolutionarily least likely mutations in the interface core still result in a minimum well in the PPI PMF, which means that some (weak) affinity is retained. This may be due to retained shape compatibility of the mutant interface or due to favourable ‘supporting’ interactions of residues in the interface rim. This could also explain our finding that least likely mutations that are performed only on one side of the interface (see SI Table 5) have much smaller disruptive effects on the binding.

We also noticed that some outer interface rim mutations significantly lower the well depth; note that these residues do not participate in the interaction in the wild-type complex. This increased binding strength could be caused by additional interactions that are introduced by these mutations. We found that the most significantly increased binding strength occurred in mutants with a higher net charge. This could mean that either additional salt-bridges are contributing to the binding, or that possibly (additional) counter-ions interact at the interface to increase the binding strength. Alternatively, the interface rim is known to

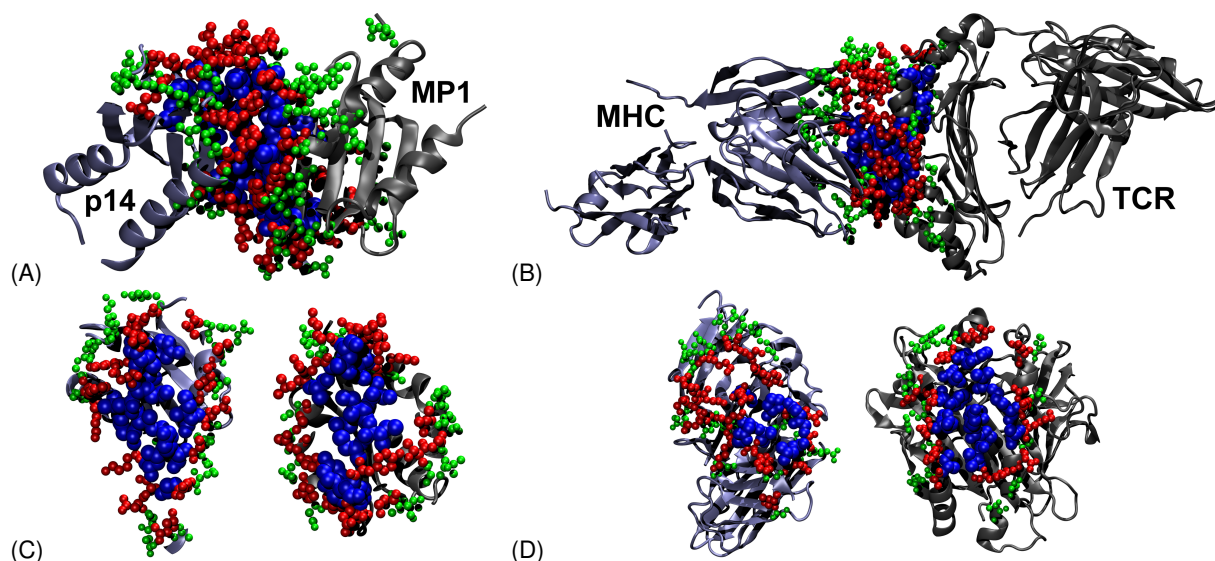


Fig. 3. Detailed view of the interface regions of interacting proteins. (A) MP1-p14 and (B) TCR-pMHC showing the interface core residues in blue, interface rim in red and outer interface rim in green in VDW representation. The rest of the proteins is shown as cartoons. (C) and (D) show the interfaces ‘opened up’ by rotation outward by 90° around the vertical axes to expose the interacting ‘faces’ (same colouring as in (A) and (B)).

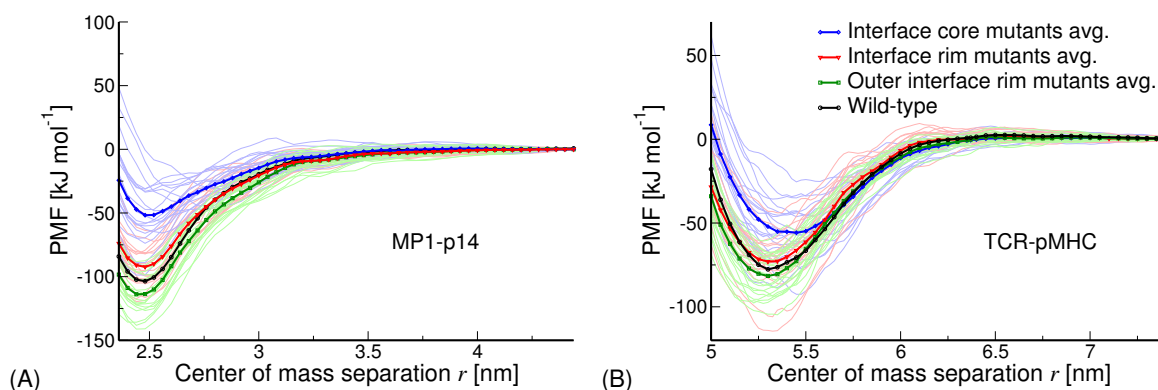


Fig. 4. The effect of mutations in different regions of the interacting pairs. The interface core mutants are in blue, interface rim in red, outer interface rim in green and the WT in black. Pale colours on the background are for each individual mutant and darker colours indicate the mean PMF for each mutant class. (A) MP1-p14 and (B) TCR-pMHC complex. SI Fig. 5 shows corresponding plots with only one out of three residues mutated.

infer specificity through complementarity of shape and binding properties (Guharoy and Chakrabarti, 2005), and is therefore not tuned for optimal binding strength. Likewise, the interface as a whole may not be evolutionarily optimised for binding affinity, as other functional aspects are also likely to give selective advantages. This means that there may in fact be ample room for optimisation of the binding affinity in any particular naturally occurring protein-protein interface.

Finally, we do see qualitative differences between the atomistic and CG PMFs, although our set of two complexes does not allow us to decide which one is in better agreement with experimental dissociation constants. Underlying reasons for these differences are likely related to the different parametrisation of short-range interactions in these force fields. The difference between the experimental and computed equilibrium distances can have a number of explanations. The crystal structures represent vacuum

systems in which the protein structure is very rigid, whereas we simulated systems of solvated ‘breathing’ proteins. Furthermore, the MARTINI forcefield includes restraints on the tertiary structure of the protein, while the unrestrained atomistic simulations will allow larger deviations in the interface upon binding. This may explain why equilibrium binding distance in the CG calculations is closer to the crystal structure than the atomistic simulations. In any case, a comparison of the experimental equilibrium COM distances to the ones we computed is expected to yield differences.

Sampling is crucial

Surprisingly, for both complexes the CG model appears to be at least as accurate in approximating the experimental value as the atomistic model. Part of the reason for that could be better sampling of the mean force for the CG model where the faster simulations enabled us to perform 20 independent simulations for each

separation distance, whereas only 3 (TCR-pMHC) or 10 (MP1-p14) simulations could realistically be performed for the atomistic model.

We also find that, for a given separation distance, simulations from slightly different starting conditions do not converge to quite the same value of the constraint force (see Fig. 1A & B, * and \circ symbols) for both the CG and the atomistic models, and this effect is strongest at short separation distances. We attribute this observation to the complex potential energy surface at small separation distances. Simulations of biomolecules starting from nearly identical initial conditions are known to get trapped in local minima (Luo *et al.*, 2006). In general, this can be overcome as well with sufficient sampling.

The reason we could perform so many more simulations for the CG model is of course its increased computational efficiency, 500 to 600 times faster than the atomistic simulations. The primary reason for this large computational gain is the reduction in particle density, and the ensuing quadratic decrease in numbers of pairwise interactions calculated. Moreover, the larger, heavier particles with softer interaction potentials in the CG force-field allow much longer integration time-steps without loss of accuracy than is possible with the atomistic force field. We can therefore conclude that, for all but very small-scale analyses, the amount of sampling required for accurate determination of the ΔG^{off} barrier can only realistically be achieved using coarse-grained models.

Some further efficiency could possibly be gained by optimising simulation parameters, particularly the integration time-step. For the atomistic simulations, time steps of up to $\Delta t=5$ or 6 fs may be used with negligible loss of accuracy (Feenstra *et al.*, 1999). A similar speedup may likewise be achieved in the CG simulations.

One final challenge regarding the accurate calculation of the free energy of binding in particular remains largely open: that of the accurate estimation of loss of rotational entropy upon formation of a protein complex (e.g. Tamura and Privalov, 1997; Yu *et al.*, 2001; Grunberg *et al.*, 2006; Chang *et al.*, 2008). In the results presented here, at 2 ns sampling, the rotational entropy is not fully sampled (see SI Fig. 4). For the free energy difference between the bound state and the unbound state, this would result in a discrepancy between the simulation and the experiment. However, at the top of the barrier this error is expected to be much smaller (Cuendet and Michielin, 2008); our $2\mu\text{s}$ simulations for the MP1-p14 complex confirm that this effect can indeed be extremely small. Furthermore, the correction is expected to be independent of the details of the force field used, and therefore we can directly compare the results between the atomistic and CG simulations.

It is interesting to note that we could use the increased efficiency in the CG simulations to directly sample rotational degrees of freedom, as indicated by the complete loss of orientational ordering at $2\mu\text{s}$ and large separation distance (see SI Fig. 4). It is beyond the scope of this work, but once sufficient sampling is established, these results can be used to estimate directly the changes in entropy during the bound to unbound transition in complexes like this one.

Limitations of the Approach

In this paper, we compared two force fields on two complexes of known structure. We have shown that for these two complexes the interaction profiles are highly similar when comparing the atomistic force field to the coarse-grained MARTINI force field. To claim generality of these findings, a larger test set may be

required. However, the computational requirement for the reference simulations using the atomistic force field is prohibitive. Note as well that none of the current methods in docking or simulation can predict binding affinities without knowledge of the bound structure (Kastritis and Bonvin, 2010).

The comparison has been made by assuming that conformations in the free state as well as in the bound state are relatively stable. For other complexes this may be different, for example when the PPI involves ‘induced fit’ effects, especially for highly flexible binding partners. It is unlikely that the methods proposed here will be directly applicable to such cases. It should be emphasised that the atomistic approach is equally unfeasible here, but in that case due to limits in computational sampling. The *in silico* mutational study presented here did not account for the possibility that mutations might disrupt protein secondary structure, since these kinds of structural rearrangements are not possible in the MARTINI model.

Future implications

Our results confirm the dominance of the interface region in determining the protein-protein interaction for the two complexes. This opens the possibility to restrict the simulated system to the interface area and intervening water only. When only a limited volume at the interface region is simulated, however, the number of water molecules in that volume cannot be assumed constant during force calculation. Rather, this system should be considered at a constant chemical potential (μ) with fluctuating numbers of particles (N), i.e. the grand-canonical (GC) or μVT ensemble.

Traditionally, MD simulations are performed in the micro-canonical (NPE), canonical (NVT), or isothermal/isobaric (NPT) ensemble, as this simplifies calculations and the complexity of the software required (Frenkel and Smit, 2002). We have recently published a python library interface to the GROMACS simulation engine (Pool *et al.*, 2012) that enables simulation of a GC μVT ensemble through a hybrid MD/Monte Carlo integration scheme.

The combined speedup achieved by coarse-graining and volume restriction would be sufficient to incorporate the calculation of binding free energies into a three-stage approach to PPI calculation for genomic-scale application. First, non-interacting protein pairs would be filtered out using cheap sequence-based methods (e.g., Ezkurdia *et al.*, 2009). Second, docking will be used to find the most likely binding interfaces (Pons *et al.*, 2010; Lensink and Wodak, 2010). In a final step, binding energy calculation will then be used to select the stable complexes (Pool and Bolhuis, 2010). While this goal, for now, remains in the future it does seem only a few small steps away.

ACKNOWLEDGEMENTS

We thank Qingzhen Hou for help with the MARTINI simulations. We thank the anonymous reviewers for helpful suggestions

Funding: This work was part of the BioRange programme of the Netherlands Bioinformatics Centre (NBIC), which is supported by a BSIK grant through the Netherlands Genomics Initiative (NGI). This work is partly financed by the Netherlands Organisation for Scientific Research (NWO). We thank SURFsara (www.surfsara.nl) for the support in using the Lisa Compute Cluster.

REFERENCES

- Berendsen, H. J. C., Postma, J. P. M., van Gunsteren, W. F., DiNola, A., and Haak, J. R. (1984). Molecular dynamics with coupling to an external bath. *J. Chem. Phys.*, **81**(8), 3684.
- Chang, C. E., McLaughlin, W. A., Baron, R., Wang, W., and McCammon, J. A. (2008). Entropic contributions and the influence of the hydrophobic environment in promiscuous protein-protein association. *Proc. Natl. Acad. Sci. U.S.A.*, **105**(21), 7456–7461.
- Cheng, A. and Merz, K. M. (1996). Application of the Nosé-Hoover chain algorithm to the study of protein dynamics. *The Journal of Physical Chemistry*, **100**(5), 1927–1937.
- Cuendet, M. A. and Michielin, O. (2008). Protein-protein interaction investigated by steered molecular dynamics: the TCR-pMHC complex. *Biophys. J.*, **95**(8), 3575–3590.
- Cui, Q., Sulea, T., Schrag, J. D., Munger, C., Hung, M. N., Nam, M., Cygler, M., and Purisima, E. O. (2008). Molecular dynamics-solvated interaction energy studies of protein-protein interactions: the MP1-p14 scaffolding complex. *J. Mol. Biol.*, **379**(4), 787–802.
- Davis-Harrison, R., Insaiddo, F., and Baker, B. (2007). T cell receptor binding transition states and recognition of peptide/mhc. *Biochemistry*, **46**, 1840–1850.
- Ding, Y., Baker, B., Garboczi, D., Biddison, W., and Wiley, D. (1999). Four α -tcr/peptide/hla-a2 structures that generate very different t cell signals are nearly identical. *Immunity*, **11**(1), 45–56.
- Dror, R. O., Dirks, R. M., Grossman, J., Xu, H., and Shaw, D. E. (2012). Biomolecular simulation: A computational microscope for molecular biology. *Annual Review of Biophysics*, **41**(1), 429–452. PMID: 22577825.
- Ezkurdia, I., Bartoli, L., Fariselli, P., Casadio, R., Valencia, A., and Tress, M. (2009). Progress and challenges in predicting protein-protein interaction sites. *Brief. Bioinformatics*, **10**(3), 233–246.
- Feenstra, K. A., Hess, B., and Berendsen, H. J. C. (1999). Improving efficiency of large time-scale molecular dynamics simulations of hydrogen-rich systems. *J. Comput. Chem.*, **20**, 786–798.
- Fennell, C. J. and Dill, K. A. (2011). Physical modeling of aqueous solvation. *Journal of Statistical Physics*, **145**, 209–226.
- Frenkel, D. and Smit, B. (2002). *Understanding molecular simulation: from algorithms to applications*. Academic Pr, San Diego, 2nd ed. edition.
- Garboczi, D. N., Ghosh, P., Utz, U., Fan, Q. R., Biddison, W. E., and Wiley, D. C. (1996). Structure of the complex between human t-cell receptor, viral peptide and hla-a2. *Nature*, **384**, 134–141.
- Gilson, M. K., Given, J. A., Bush, B. L., and McCammon, J. A. (1997). The statistical-thermodynamic basis for computation of binding affinities: a critical review. *Biophys. J.*, **72**(3), 1047–1069.
- Grunberg, R., Nilges, M., and Leckner, J. (2006). Flexibility and conformational entropy in protein-protein binding. *Structure*, **14**(4), 683–693.
- Guharoy, M. and Chakrabarti, P. (2005). Conservation and relative importance of residues across protein-protein interfaces. *Proc. Natl. Acad. Sci. U.S.A.*, **102**(43), 15447–15452.
- Hadley, K. R. and McCabe, C. (2012). Coarse-grained molecular models of water: a review. *Molecular Simulation*, **38**(8-9), 671–681.
- Henikoff, S. and Henikoff, J. G. (1992). Amino acid substitution matrices from protein blocks. *Proc. Natl. Acad. Sci. U.S.A.*, **89**(22), 10915–10919.
- Hess, B., Kutzner, C., van der Spoel, D., and Lindahl, E. (2008). Gromacs 4: Algorithms for highly efficient, load-balanced, and scalable molecular simulation. *J. Chem. Theory Comput.*, **4**(3), 435–447.
- Homeyer, N. and Gohlke, H. (2012). Free energy calculations by the molecular mechanics poisson-boltzmann surface area method. *Molecular Informatics*, **31**(2), 114–122.
- Humphrey, W., Dalke, A., and Schulten, K. (1996). VMD – Visual Molecular Dynamics. *Journal of Molecular Graphics*, **14**, 33–38.
- Kabsch, W. and Sander, C. (1983). Dictionary of protein secondary structure: Pattern recognition of hydrogen-bonded and geometrical features. *Biopolymers*, **22**, 2577–2637.
- Kastritis, P. and Bonvin, A. (2010). Are scoring functions in protein-protein docking ready to predict interactomes? Clues from a novel binding affinity benchmark. *J. Proteome Res.*, **9**(5), 2216–2225.
- Kurzbaue, R., Teis, D., de Araujo, M. E. G., Maurer-Stroh, S., Eisenhaber, F., Bourenkov, G. P., Bartunik, H. D., Hekman, M., Rapp, U. R., Huber, L. A., and Clausen, T. (2004). Crystal structure of the p14/mp1 scaffolding complex: How a twin couple attaches mitogen-activated protein kinase signaling to late endosomes. *Proc. Natl. Acad. Sci. U.S.A.*, **101**(30), 10984–10989.
- Lensink, M. and Wodak, S. (2010). Blind predictions of protein interfaces by docking calculations in capri. *Proteins*, **78**(15), 3085–3095.
- Luo, G., Andricioaei, I., Xie, X. S., and Karplus, M. (2006). Dynamic distance disorder in proteins is caused by trapping. *J. Phys. Chem. B*, **110**(19), 9363–9367.
- Marrink, S. J., Risselada, H. J., Yefimov, S., Tieleman, D. P., and de Vries, A. H. (2007). The martini force field: coarse grained model for biomolecular simulations. *J. Phys. Chem. B*, **111**(27), 7812–24.
- Mizuguchi, K., Deane, C. M., Blundell, T. L., Johnson, M. S., and Overington, J. (1998). Joy: protein sequence-structure representation and analysis. *Bioinformatics*, **14**(7), 617–623.
- Monticelli, L., Kandasamy, S. K., Periole, X., Larson, R. G., Tieleman, D. P., and Marrink, S.-J. (2008). The martini coarse-grained force field: Extension to proteins. *J. Chem Theory Comput.*, **4**(5), 819–834.
- Ofran, Y. and Rost, B. (2007). Protein-protein interaction hotspots carved into sequences. *PLoS Comput. Biol.*, **3**(7), e119.
- Oshima, H., Yasuda, S., Yoshidome, T., Ikeguchi, M., and Kinoshita, M. (2011). Crucial importance of the water-entropy effect in predicting hot spots in protein-protein complexes. *Phys Chem Chem Phys*, **13**(36), 16236–16246.
- Parrinello, M. and Rahman, A. (1981). Polymorphic transitions in single crystals: A new molecular dynamics method. *Journal of Applied Physics*, **52**(12), 7182–7190.
- Periole, X., Knepp, A. M., Sakmar, T. P., Marrink, S. J., and Huber, T. (2012). Structural determinants of the supramolecular organization of g protein-coupled receptors in bilayers. *Journal of the American Chemical Society*, **134**(26), 10959–10965.
- Pons, C., Grosdidier, S., Solernou, A., Perez-Cano, L., and Fernandez-Recio, J. (2010). Present and future challenges and limitations in protein-protein docking. *Proteins*, **78**(1), 95–108.
- Pool, R. and Bolhuis, P. G. (2010). The influence of micelle formation on the stability of colloid surfactant mixtures. *Phys Chem Chem Phys*, **12**, 14789–14797.
- Pool, R., Heringa, J., Hoefling, M., Schulz, R., Smith, J. C., and Feenstra, K. A. (2012). Enabling grand-canonical monte carlo: Extending the flexibility of gromacs through the grompy python interface module. *Journal of Computational Chemistry*, **33**(12), 1207–1214.
- Sali, A. and Blundell, T. L. (1993). Comparative protein modelling by satisfaction of spatial restraints. *Journal of molecular biology*, **234**(3), 779–815.
- Schueler-Furman, O., Wang, C., Bradley, P., Misura, K., and Baker, D. (2005). Progress in modeling of protein structures and interactions. *Science*, **310**(5748), 638–642.
- Sprinzak, E., Sattath, S., and Margalit, H. (2003). How reliable are experimental protein-protein interaction data? *J. Mol. Biol.*, **327**(5), 919–923.
- Tamura, A. and Privalov, P. L. (1997). The entropy cost of protein association. *J. Mol. Biol.*, **273**(5), 1048–1060.
- Tobi, D. (2010). Designing coarse grained-and atom based-potentials for protein-protein docking. *BMC Struct. Biol.*, **10**, 40.
- Trzesniak, D., Kunz, A.-P. E., and van Gunsteren, W. F. (2007). A comparison of methods to compute the potential of mean force. *ChemPhysChem*, **8**(1), 162–169.
- Tuffery, P. and Derreumaux, P. (2012). Flexibility and binding affinity in protein-ligand, protein-protein and multi-component protein interactions: limitations of current computational approaches. *Journal of The Royal Society Interface*, **9**(66), 20–33.
- Tuncbag, N., Kar, G., Keskin, O., Gursoy, A., and Nussinov, R. (2009). A survey of available tools and web servers for analysis of protein-protein interactions and interfaces. *Brief. Bioinformatics*, **10**(3), 217–232.
- van Gunsteren, W. F., Billeter, S. R., Eising, A. A., Hünenberger, P. H., Krüger, P. A., Mark, E., Scott, W. R. P., and Tironi, I. G. (1996). *Biomolecular Simulation: The GROMOS96 Manual and User Guide*. Vdf Hochschulverlag AG an der ETH Zürich, Zürich, Switzerland.
- Wereszczynski, J. and McCammon, J. A. (2012). Statistical mechanics and molecular dynamics in evaluating thermodynamic properties of biomolecular recognition. *Quarterly Reviews of Biophysics*, **45**, 1–25.
- Wollacott, A., Zanghellini, A., Murphy, P., and Baker, D. (2007). Prediction of structures of multidomain proteins from structures of the individual domains. *Protein Sci.*, **16**(2), 165–175.
- Wu, L. C., Tuot, D. S., Lyons, D. S., Garcia, K. C., and Davis, M. M. (2002). Two-step binding mechanism for T-cell receptor recognition of peptide MHC. *Nature*, **418**(6897), 552–556.
- Yu, Y. B., Privalov, P. L., and Hodges, R. S. (2001). Contribution of translational and rotational motions to molecular association in aqueous solution. *Biophys. J.*, **81**(3), 1632–1642.